

Unidirectional Synchronization of Silicon Optomechanical Nanobeam Oscillators by External Feedback

David Alonso-Tomás, Néstor E. Capuj, Laura Mercadé, Amadeu Griol, Alejandro Martínez, and Daniel Navarro-Urrios*



Cite This: *ACS Photonics* 2024, 11, 7–12



Read Online

ACCESS |

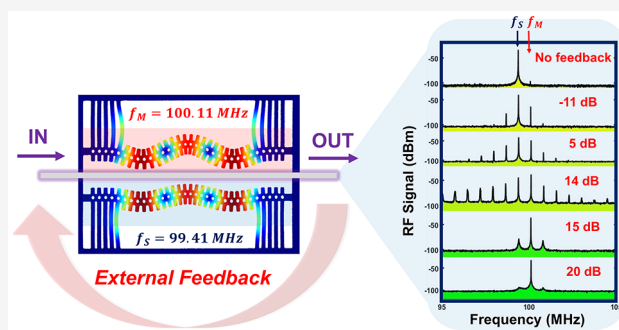
Metrics & More

Article Recommendations

Supporting Information

ABSTRACT: The remote synchronization of oscillators is essential for improving the performance, efficiency, and reliability of various systems and technologies, ranging from everyday telecommunications to cutting-edge scientific research and emerging technologies. In this work, we unequivocally demonstrate a unidirectional type of synchronization between two self-sustained optomechanical crystal oscillators that interact solely through an external optical feedback stage. Several pieces of experimental evidence rule out the possibility of resonant forcing and, in contrast to previous works, indicate that synchronization is achieved in the regime of natural dynamics suppression. Our experimental results are in agreement with the predictions of a numerical model describing the specific mechanical lasing dynamics of each oscillator and the unidirectional interaction between them. The outcomes of our study pave the way toward the synchronization of clock signals corresponding to far-placed processing elements in a future synchronous photonic integrated circuit.

KEYWORDS: *synchronization, cavity optomechanics, silicon photonics, nonlinear dynamics, photonic crystals*



INTRODUCTION

Synchronization is the term used to describe the coordination of the temporal dynamics of two or more self-sustained oscillators by means of a weak interaction.¹ First proposed by Lord Huygens in the 17th century,² this phenomena has been widely found throughout Nature from the microscopic to macroscopic world.^{3–7} Unsurprisingly, synchronization, either unidirectional or bidirectional, has garnered significant interest in the last decades being applied in signal-processing,⁸ RF communications,⁹ clock synchronization,¹⁰ or even neural networks,¹¹ among others. With the advances in micro- and nanotechnologies, efforts have been dedicated to achieve the synchronization of self-oscillating micro- and nanoelectromechanical systems (MEMS/NEMS), which offer a robust high frequency operation, miniaturization, and great scalability.^{12–16} Optomechanical oscillators (OMOs) are a subset of MEMS/NEMS oscillators that activate large amplitude coherent mechanical motion driven by optical forces.¹⁵ OMOs are great candidates to explore synchronization mechanisms, since the interaction can be mediated by optical signals and, therefore, be effective even at large distances between nodes.^{17–20} On the other hand, there are several proposals concerning synchronization of OMOs that go from purely mechanical synchronization through a mechanical link²¹ to the use of a common optical mode that drive both oscillators^{22–24} or even an array of them.^{25,26} These alternatives provide low

scalability and would not allow synchronization on demand of distant subsystems within a complex optomechanical (OM) network.

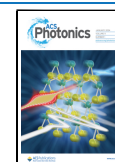
In this paper, we unequivocally demonstrate the synchronization between two OMOs based on silicon OM crystal nanobeams driven by optical forces, which are spectrally separated both in the mechanical and optical domains. Thus, even if in our experiment the OMOs are placed in the same chip, they do not interact and can be effectively considered as if they were far from each other. The synchronization scheme is a unidirectional configuration where the light modulation generated by one OMO (referred as main or primary hereon) is fed to the other one (called secondary or follower) using external circuitry. Remote synchronization of OMOs has been recently claimed in the case of circular resonators like disks, spheres, or toroids.^{17,18} In contrast to the previous geometries, our system of Si-based OM crystal nanobeams is physically connected to the rest of the chip, thus allowing for the direct extraction of coherent mechanical signals into an eventual

Received: September 29, 2023

Revised: December 21, 2023

Accepted: December 21, 2023

Published: December 27, 2023



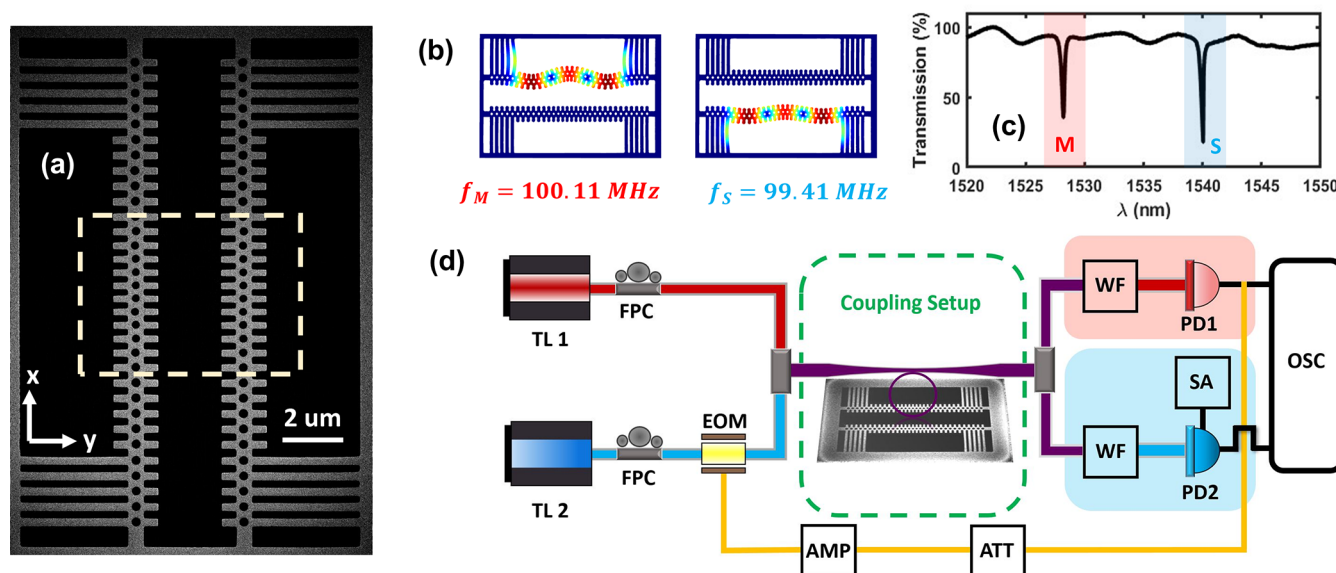


Figure 1. Characteristics of the tested optomechanical crystal cavities and experimental setup. (a) SEM image of a pair of integrated optomechanical cavities. Optical cavity modes lie in the highlighted region. (b) FEM simulations of the mechanical displacement field of the mechanical mode under study. This analysis utilizes a geometry imported from the SEM image of panel a. (c) Optical transmission spectra of the device under test. The red and blue shaded regions denote main and secondary OMO resonances, respectively. (d) Schematic of the experimental setup: Tunable laser (TL); Fiber polarizer controller (FPC); Tunable Fabry-Perot filter (WF); Photodetector (PD); Spectrum analyzer (SA); Oscilloscope (OSC); Attenuator (ATT); Amplifier (AMP); Electro-optic modulator (EOM). Red and blue paths indicate the different laser wavelengths necessary to excite the main and secondary oscillator resonances, respectively. Purple path indicates the zones where both wavelengths propagate simultaneously.

phononic circuit. Furthermore, the route toward synchronization is performed in the regime of suppression of the natural dynamics described by Balanov¹ instead of the phase-locking mechanisms explored in previous literature.^{17,18,27} Finally, we rule out the possibility of resonant forcing of the secondary OMO, which has been overlooked in the past.

An essential condition for synchronization between two oscillators is that both of them should be self-sustained.^{1,7,13} This means that, in each oscillator, gain overcomes mechanical losses, and the mechanical motion becomes coherent and of large amplitude. This regime will be referred to hereon as mechanical lasing given its similarity with the optical counterpart, and the OM crystal nanobeams will be treated as OMOs. The OM crystals under study are driven to the mechanical lasing regime using a self-pulsing (SP) mechanism that has been extensively explored elsewhere^{28–30} and in our group^{31,32} in the sideband unresolved regime. It is based on the anharmonic modulation of the radiation pressure force induced by the dynamical self-limit cycle generated between free-carrier dispersion (FCD) and the thermo-optic (TO) effect in silicon. Essentially, these effects produce a modulation of the refractive index of the material and, therefore, a movement of the cavity resonance at a certain frequency (ν_{sp}). When a harmonic (M) of ν_{sp} is partially resonant with a mechanical mode of the structure, it can provide coherent amplification and drive it to the mechanical lasing regime. The SP frequency can be thermally tuned in the tens of MHz range by increasing the average intracavity photon number (n_0) so that the cavity is heated up (see Supporting Information, S2).

TESTED DEVICE AND EXPERIMENTAL SETUP

The device investigated here is composed of a pair of integrated nominally identical one-dimensional OM crystal cavities, which have been fabricated using standard Si

nanofabrication techniques on a silicon-on-insulator wafer (see Supporting Information, S1). The outermost five cells on each side of the OM crystals are anchored with tethers to the partially underetched Si frame (Figure 1a). This arrangement ensures that the flexural modes within the plane are isolated from the frame and restricted to the central area of the cavities, which are specifically engineered to sustain high quality factor optical modes for transversal electric (TE) polarization around $1.53 \mu\text{m}$.³³ Both cavities are separated by $2 \mu\text{m}$ in such a way that it is possible to optically excite them simultaneously by placing a single tapered fiber in between. Although these geometries are nominally identical, fabrication imperfections produce slightly different mechanical and optical resonant frequencies. In particular, the mechanical modes used in this work correspond to the in-plane flexural ones having three antinodes along the x direction and mechanical frequencies of $(f_m, f_s) = (\Omega_m, \Omega_s)/2\pi = (100.11, 99.41) \text{ MHz}$, where the subindices m and s denote main and secondary oscillators, respectively (Figure 1b). The transmission spectrum of the whole device is obtained by performing a sweep in wavelength for low input power ($P_{in} = 0.5 \text{ mW}$), which results in two well-separated optical resonances at $(\lambda_m, \lambda_s) = (1528.20, 1540.05) \text{ nm}$, holding an overall quality factor of $Q_{m,s} = (5.68, 6.67) \times 10^3$, respectively (Figure 1c). It is worth noting that separated optical resonances are essential to avoid optical cross-talk between the OMOs.

Figure 1d shows the setup used to perform the experiment. To achieve the simultaneous optical excitation of both OMOs we employ two tunable lasers, each one tuned at the resonant wavelength of its corresponding OMO. The polarization of each laser is controlled to be TE, which matches that of the cavity modes. Light of the two lasers is afterward combined and driven to a microloop-shaped fiber that has been thinned down to a diameter of about $1.5 \mu\text{m}$. The bottom part of the

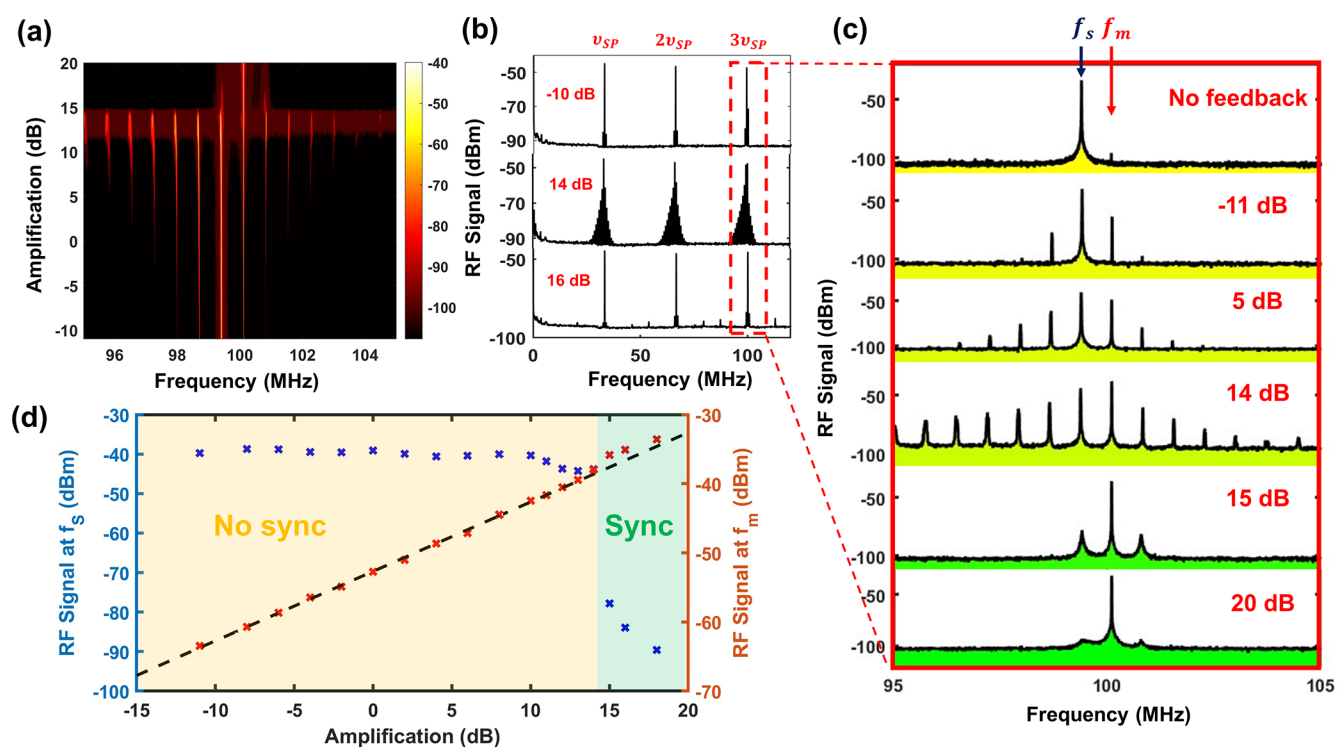


Figure 2. Radio frequency (RF) analysis of the light transmission modulated by the secondary OMO dynamics detected at PD2. (a) Contour RF plot near the mechanical natural frequency of the oscillator as a function of the amplification provided by the feedback stage (AMP+ATT) to the signal coming from PD1 before being introduced in the EOM (see Figure 1d). (b) Wider RF spectrum for different amplification power. Note that $M = 3$ dynamics is present as two extra peaks at one- and two-thirds of the natural frequency of oscillation. (c) Magnification around the natural resonance of the secondary cavity. No feedback indicates the situation in which the amplification stage is not present in the setup. (d) Amplitude of the RF signal at the secondary (blue) and main (red) oscillators' natural frequency, represented as a function of the feedback amplification.

microloop can act as a probe that enables the local excitation of the optical cavity modes when the cavities are placed in the near field region of the fiber. Then, light is divided in two paths and spectrally filtered by tunable fabry-perot filters (WF) to record the laser wavelengths resonant with the main and secondary OMOs in photodetectors PD1 and PD2, respectively. The secondary oscillator signal is derived from a spectrum analyzer (SA) while the main one is introduced as a modulation feedback on the laser exciting the second cavity by means of an electro-optic modulator (EOM) with a half-wave voltage $V_{\pi} = 3.5$ V. The offset voltage is set near the quadrature point $V_{DC} = 0.5 V_{\pi}$ so that if the RF modulation signal is small, the output light power responds linearly (see Supporting Information, S3). The magnitude of the feedback signal and, consequently, the modulation amplitude of the second laser (TL2) are governed by a stage that allows for tunable attenuation or amplification. As a result of this experimental configuration, the external feedback is the only interaction between both OMOs. Thus, even if the two OMOs are physically placed close to each other, the system is equivalent to have them separated in space. Finally, both detector output signals are temporally analyzed in a 4-channel oscilloscope (OSC).

RESULTS AND DISCUSSION

By using the SP mechanism explained above, both cavities are excited to different mechanical lasing regimes: $M = 3$ for the case of the secondary OMO (where the third harmonic of the SP oscillating at a frequency of $3\nu_{SP}$ is providing the mechanical amplification) and $M = 1$ for the main one. This

mechanical lasing scheme allows the clear distinguishing between a forcing mechanism and unidirectional synchronization since the differences may be subtle. Indeed, the modulation feedback generated by the primary oscillator could resonantly drive the follower, while eliminating its self-sustained mechanical oscillation. This would obviously lead to a mechanical oscillation that would be coherent with that of the main OMO, which may be confused with synchronization. By keeping an $M = 3$ regime in the secondary oscillator throughout the whole set of measurements we ensure the distinction between both possibilities, since in the case of resonant forcing, the oscillations corresponding to SP dynamics at ν_{SP} and $2\nu_{SP}$ would disappear. Figure 2a shows the RF response of the secondary OMO in a 10 MHz spectral window around the mechanical resonance when varying the feedback amplification. Note that this value is quantified in a logarithmic scale which represents the amplification that the output signal of PD1 receives before modulating the TL2 path through the EOM. As the top panel of Figure 2b shows, when the feedback signal is attenuated before entering the EOM (-10 dB), the secondary oscillator presents three RF peaks at frequencies $\nu_{SP} = f_s/3$, $2\nu_{SP} = 2f_s/3$, and $3\nu_{SP} = f_s$, which corresponds to the behavior expected due to the resonant driving provided by the third harmonic of the SP mechanism. As the feedback modulation amplitude is increased, sidebands resulting from the coherent sum of both nonlinear oscillations (secondary oscillator and modulation harmonics from the feedback) appear at various possible combination of their frequencies. Synchronization is observed above a certain amplification threshold value of 15 dB, given that the mechanical frequency of the secondary oscillator (f_s) is locked

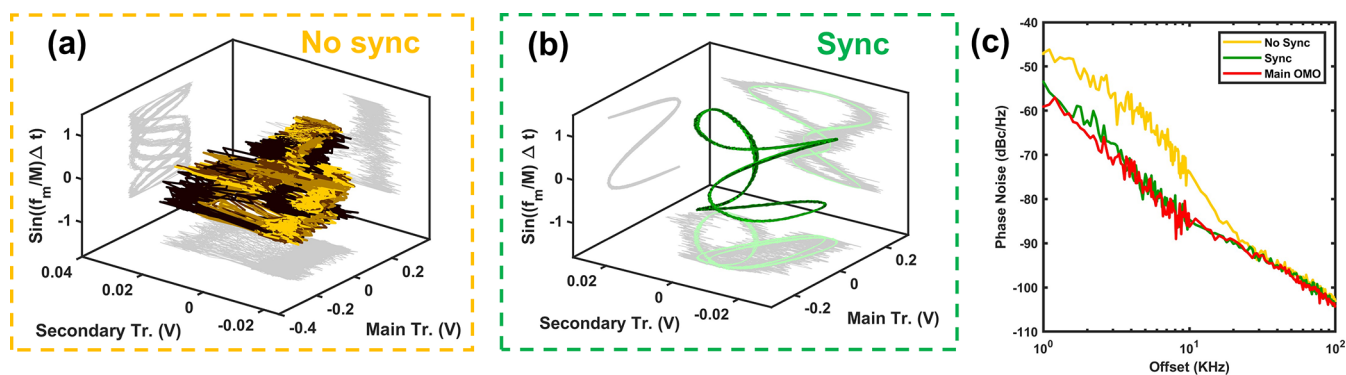


Figure 3. Temporal dynamics and phase noise of OM oscillators in the synchronization and free running regime. (a) Poincaré map of the recorded temporal traces of the free running secondary OMO using a stroboscopic technique with a sampling frequency of $f_m/3$. Each colored curve corresponds to a different value of the initial delay (Δt). Projections in the different two-dimensional planes are shown in gray. (b) Same representation for the case when the feedback amplification is above the synchronization threshold (20 dB). A fit (green) is performed to the raw data of the secondary oscillator (gray). (c) Phase noise measured on the natural frequency of oscillation of the main (red) and secondary (yellow) OMOs detected at PD1 and PD2, respectively, for the case where no feedback is applied. The green curve corresponds to the same measurement on the secondary OMO RF signal after the threshold of synchronization (>15 dB). Horizontal axis indicates the frequency offset.

to that of the main one (f_m) and most of the sidebands disappear. Two wide sidebands remain at a beating frequency of $(f_m - f_s)$, which are clear signatures of unidirectional synchronization that have been reported in previous works addressing synchronization of photonic cavities.²³ Their origin lies in the thermal force noise acting on the secondary OMO, which tends to push away its dynamics from the synchronization limit cycle. These experimental results have been compared with numerical simulations performed using a model based on the SP equations coupled to harmonic mechanical oscillators, showing a good qualitative agreement (see Supporting Information, S3). The measured synchronization mechanism resembles the suppression of the natural dynamics route described by Balanov¹ for a Van der Pol self-sustained oscillator under the actuation of a harmonic external force. Under this mechanism, the synchronization region is entered at relatively large amplitudes of forcing in comparison to a phase-locking mechanism, with one of the main characteristics of its route being the absence of frequency pulling. Indeed, synchronization by suppression appears if the separation between the natural frequencies of the oscillators is rather large, which is indeed our case ($\Delta f = 0.7$ MHz, i.e., about 0.7%). Note that the threshold of 15 dB roughly corresponds to a modulation amplitude of 60% (see Supporting Information, S3), which is 1 order of magnitude larger than in the case of the phase-locking mechanism explored in previous works on the same type of OMOs.²⁷ Regarding the bottom panel of Figure 2b (16 dB), it is observed that the $M = 3$ mechanical lasing secondary oscillator dynamics is preserved even after the threshold for synchronization. In fact, the first and second harmonics of self-pulsing oscillate now at one- and two-thirds of the frequency of the main OMO signal (see Supporting Information, S4). Thus, as mentioned earlier, this is evidence that the follower oscillator is just adapting its dynamics to synchronize with the modulation generated by the main one and hence discards resonant forcing. It is worth noting that, by definition, a resonant forcing induces an oscillation at the frequency of the driving signal. Therefore, in that case, we would observe that the first RF peak would be placed at f_m (not at $f_m/3$, as it is observed after synchronization) and would be associated only to the forced mechanical oscillation of the secondary cavity, since the self-

pulsing oscillator would stop existing. These experimental observations demonstrate that, after the transition, the self-pulsing is still active and, therefore, keeps being the main driving source of the mechanical oscillation of the secondary OMO (as it was just before the threshold). The intensity of the RF peaks appearing in the secondary oscillator signal at the natural frequencies of each OMO is analyzed in Figure 2d as a function of the feedback stage amplification. As expected, the RF peak associated with the secondary oscillator remains relatively constant until it sharply declines after synchronization, with a reduction of about 34 dB in the RF signal at f_s . In the case of the main OMO RF peak there is a linear relation with feedback amplification with a slope near to one, which indicates that the response of the modulation amplitude to the amplification/attenuation stage is linear. Interestingly, this linear tendency is altered with an abrupt increase of the RF peak signal when the transition to synchronization occurs. This effect is linked to the transfer of self-sustained oscillation energy from the secondary oscillator natural frequency to the main one, further confirming synchronization rather than forced oscillation. Before synchronization (in the 11–14 dB range), there is a transient regime where the RF signal at f_s reduces its amplitude until becoming 4 times smaller than the one corresponding to f_m . This illustrates the naming of the synchronization mechanism, since the external modulation is suppressing the natural dynamics of the oscillator without forcing it. It is also worth mentioning that, as shown in the top spectra of Figure 2c, even in the absence of external feedback, there is a weak RF peak corresponding to the dynamics of the primary oscillator, which is associated with a subtle mechanical cross-talk between the OMOs through the frame surrounding them. This interaction, in addition to being negligible compared to the amplitude of the lasing mechanical motion, is not in phase with the one introduced in the secondary OMO using the external feedback mechanism. Therefore, its contribution to the synchronization mechanism can be neglected.

The temporal behavior of the transmitted signals of both OMOs has been analyzed in the oscilloscope by recording traces of 800 ns using the secondary OMO signal as the trigger. Figure 3a,b shows the data represented as a Poincaré map, where the z-axis has been chosen to be $\sin\left(\frac{2\pi\Omega_m}{3}\Delta t\right)$ to

illustrate the trajectory in a three-dimensional space. Below the synchronization threshold (Figure 3a), most of the phase space is filled by the traces, which is a clear indication that the secondary and main signals are not in sync. On the other hand, when synchronization occurs, the trajectory follows a closed curve in the phase diagram (Figure 3b). A fit was performed to the oscillation trace of the follower oscillator to clearly observe the trajectory of the cycle. Finally, the phase noise of the free running and synchronized secondary OMO is reported and compared with that of the main oscillator. Figure 3c shows the results of this analysis. The phase noise of the main OMO is displayed in a range between 1 and 100 kHz of frequency offset (red curve in Figure 3c). Obviously, the curve is independent of the amplification value and exhibits a value of -85 dBc/Hz at 10 kHz. Regarding the secondary OMO, the situation in which no feedback is applied to the TL2 path (yellow curve of Figure 3c) displays a larger phase noise in comparison to that of the main OMO, i.e., -75 dBc/Hz at 10 kHz. When an external feedback above the synchronization threshold is applied (amplification = 15 dB), the phase noise curve of the signal detected at PD2 (green curve of Figure 3c) now resembles the one of the main OMO, thus improving its performance at low frequencies. Note that this noise reduction is possible since the main oscillator exhibits lower phase noise. In any case, the main conclusion of this analysis is that, above the synchronization threshold, both oscillators exhibit similar phase noise curves. This result aligns with the rest of the experimental measurement performed in the work and constitutes another proof of synchronization between the OMOs. In the region in between the two extreme situations reported, there is a strong increase of the phase noise as we approach the synchronization transition (not shown) partly associated with the presence of all the sidebands observed in Figure 2a. After the synchronization transition, the noise becomes similar to that of the main oscillator, without any noticeable change with the amplification value.

CONCLUSION

In conclusion, a unidirectional type of synchronization between two independent 1D optomechanical cavity self-sustained oscillators has been unambiguously demonstrated by introducing an external optical feedback mechanism. The route toward synchronization has been shown to be by suppression of the natural dynamics instead of the more standard phase-locking while ruling out the possibility of resonant forcing. Furthermore, OM crystal nanobeams offer the advantage of being physically connected to the silicon-based platform, therefore enabling the extraction of mechanical signals in an efficient manner. Even though in this work the oscillators are integrated in the same platform, the synchronization achieved by this method does not depend on the distance between them. In that way, the system presented here could be upscaled to networks of optomechanical oscillators interacting remotely, so that clock signals can be distributed along the system while also serving as a platform for the study of nonlinear dynamics in complex systems.

ASSOCIATED CONTENT

Supporting Information

(PDF) The Supporting Information is available free of charge at <https://pubs.acs.org/doi/10.1021/acsp Photonics.3c01397>.

Section 1: additional details about the fabricated and simulated OM structures; Section 2: deep description of the theoretical model that describes the SP mechanism; Section 3: numerical simulations about the synchronization experiment using the theoretical model; Section 4: the mechanical lasing regime of the secondary OMO during the experiment is analyzed (PDF)

AUTHOR INFORMATION

Corresponding Author

Daniel Navarro-Urrios – MIND-IN2UB, Departament d'Enginyeria Electrònica i Biomèdica, Facultat de Física, Universitat de Barcelona, Barcelona 08028, Spain; orcid.org/0000-0001-9055-1583; Email: dnavarro@ub.edu

Authors

David Alonso-Tomás – MIND-IN2UB, Departament d'Enginyeria Electrònica i Biomèdica, Facultat de Física, Universitat de Barcelona, Barcelona 08028, Spain; orcid.org/0000-0002-7804-8720

Néstor E. Capuj – Depto. Física, Universidad de La Laguna, 38200 San Cristóbal de La Laguna, Spain; Instituto Universitario de Materiales y Nanotecnología, Universidad de La Laguna, 38071 Santa Cruz de Tenerife, Spain

Laura Mercadé – MIND-IN2UB, Departament d'Enginyeria Electrònica i Biomèdica, Facultat de Física, Universitat de Barcelona, Barcelona 08028, Spain; Nanophotonics Technology Center, Universitat Politècnica de València, 46022 Valencia, Spain

Amadeu Griol – Nanophotonics Technology Center, Universitat Politècnica de València, 46022 Valencia, Spain

Alejandro Martínez – Nanophotonics Technology Center, Universitat Politècnica de València, 46022 Valencia, Spain; orcid.org/0000-0001-5448-0140

Complete contact information is available at:

<https://pubs.acs.org/10.1021/acsp Photonics.3c01397>

Funding

This work was supported by the MICINN Projects ALLEGRO (Grant Nos. PID2021-124618NB-C22 and PID2021-124618NB-C21) and MOCCASIN-2D (Grant No. TED2021-132040B-C21). A.M. acknowledges funding from the Generalitat Valenciana under Grants IDIFEDER/2020/041 and IDIFEDER/2021/061.

Notes

The authors declare no competing financial interest.

REFERENCES

- (1) Balanov, N. J.; Postnov, D. *Synchronization: From Simple to Complex*; Springer, 2009.
- (2) Huygens, C. *Horologium Oscillatorium (The Pendulum Clock)*; Apud F. Muguet: Paris, 1673; (Translation by Blackwell, R. J.) Iowa State University Press: Ames, 1986.
- (3) Feynman, R. P. Synthetic biology: Synchronized bacterial clocks. *Phys. Rev.* **1954**, *463*, 301–302.
- (4) Hammond, C.; Bergman, H.; Brown, P. Pathological synchronization in Parkinson's disease: networks, models and treatments. *Trends. Neurosci.* **2007**, *30*, 357–364.
- (5) Glass, L. Synchronization and rhythmic processes in physiology. *Nature* **2001**, *410*, 277–284.
- (6) Lamb, K.; Aly, J.; Cook, M.; Lamb, D. Synchronization of magnetic stars in binary systems. *Astrophys. J.* **1983**, *274*, L71–75.

- (7) Pykovsky, A.; Rosenblum, M.; Kurths, J. *Synchronization: A Universal Concept in Nonlinear Sciences*; Cambridge University Press: Cambridge, England, 2003.
- (8) Heinrich, M.; Moeneclaey, M.; Fechtel, S. *Digital Communication Receivers: Synchronization, Channel Estimation and Signal Processing*; Wiley: New York, 1998.
- (9) Bregni, S. *Synchronization of Digital Telecommunications Networks*; Wiley: New York, 2002.
- (10) Rhee, I.; Lee, J.; Kim, J.; Serpedin, E.; Wu, Y. Clock Synchronization in Wireless Sensor Networks: An Overview. *Sensors* **2009**, *9* (1), 56–85.
- (11) Dörfler, F.; Bullo, F. Synchronization in complex networks of phase oscillators: A survey. *Automatica* **2014**, *50*, 1539.
- (12) Asadi, K.; Yu, J.; Cho, H. Nonlinear couplings and energy transfer in micro- and nano-mechanical resonators: intermodal coupling, internal resonance and synchronization. *Philos. Trans. Royal Soc. A* **2018**, *376*, 20170141.
- (13) Matheny, M. H.; Grau, M.; Villanueva, L. G.; Karabalin, R. B.; Cross, M. C.; Roukes, M. L. Phase Synchronization of Two Anharmonic Nanomechanical Oscillators. *Phys. Rev. Lett.* **2014**, *112*, 014101.
- (14) Holmes, C. A.; Meaney, C. P.; Milburn, G. J. Synchronization of many nanomechanical resonators coupled via a common cavity field. *Phys. Rev. E* **2012**, *85*, 066203.
- (15) Aspelmeyer, M.; Kippenberg, T. J.; Marquardt, F. Cavity optomechanics. *Rev. Mod. Phys.* **2014**, *86*, 1391–1452.
- (16) Matheny, M. H.; Grau, M.; Villanueva, L. G.; Karabalin, R. B.; Cross, M. C.; Roukes, M. L. Phase Synchronization of Two Anharmonic Nanomechanical Oscillators. *Phys. Rev. Lett.* **2014**, *112*, 014101.
- (17) Li, J.; Zhou, Z.-H.; Wan, S.; Zhang, Y.-L.; Shen, Z.; Li, M.; Zou, C.-L.; Guo, G.-C.; Dong, C.-H. All-Optical Synchronization of Remote Optomechanical Systems. *Phys. Rev. Lett.* **2022**, *129*, 063605.
- (18) Shah, S. Y.; Zhang, M.; Rand, R.; Lipson, M. Master-Slave Locking of Optomechanical Oscillators over a Long Distance. *Phys. Rev. Lett.* **2015**, *114*, 113602.
- (19) Shah, S. Y.; Zhang, M.; Rand, R.; Lipson, M. Long-range Synchronization of Nanomechanical Oscillators with Light. *arXiv:1511.08536 [physics.optics]* **2017**, na.
- (20) Jang, J. K.; Klenner, A.; Ji, X.; Okawachi, Y.; Lipson, M.; Gaeta, A. L. Synchronization of coupled optical microresonators. *Nat. Photonics* **2018**, *12*, 688.
- (21) Colombano, M. F.; Arregui, G.; Capuj, N. E.; Pitanti, A.; Maire, J.; Griol, A.; Garrido, B.; Martinez, A.; Sotomayor-Torres, C. M.; Navarro-Urrios, D. Synchronization of Optomechanical Nanobeams by Mechanical Interaction. *Phys. Rev. Lett.* **2019**, *123*, 017402.
- (22) Zhang, M.; Wiederhecker, G. S.; Manipatruni, S.; Barnard, A.; McEuen, P.; Lipson, M. Synchronization of Micromechanical Oscillators Using Light. *Phys. Rev. Lett.* **2012**, *109*, 233906.
- (23) Bagheri, M.; Poot, M.; Fan, L.; Marquardt, F.; Tang, H. X. Photonic Cavity Synchronization of Nanomechanical Oscillators. *Phys. Rev. Lett.* **2013**, *111*, 213902.
- (24) Sheng, J.; Wei, X.; Yang, C.; Wu, H. Self-Organized Synchronization of Phonon Lasers. *Phys. Rev. Lett.* **2020**, *124*, 053604.
- (25) Zhang, M.; Shah, S.; Cardenas, J.; Lipson, M. Synchronization and Phase Noise Reduction in Micromechanical Oscillator Arrays Coupled through Light. *Phys. Rev. Lett.* **2015**, *115*, 163902.
- (26) Gil-Santos, E.; Labousse, M.; Baker, C.; Goetschy, A.; Hease, W.; Gomez, C.; Lemaitre, A.; Leo, G.; Ciuti, C.; Favero, I. Light-Mediated Cascaded Locking of Multiple Nano-Optomechanical Oscillators. *Phys. Rev. Lett.* **2017**, *118*, 063605.
- (27) Arregui, G.; Colombano, M. F.; Maire, J.; Pitanti, A.; Capuj, N. E.; Griol, A.; Martínez, A.; Sotomayor-Torres, C. M.; Navarro-Urrios, D. Injection locking in an optomechanical coherent phonon source. *Nanophotonics* **2021**, *10*, 1319–1327.
- (28) Johnson, T. J.; Borselli, M.; Painter, O. Self-induced optical modulation of the transmission through a high-Q silicon microdisk resonator. *Opt. Express* **2006**, *14*, 817–831.
- (29) Borghi, M.; Bazzanella, D.; Mancinelli, M.; Pavesi, L. On the modeling of thermal and free carrier nonlinearities in silicon-on-insulator microring resonators. *Opt. Express* **2021**, *29*, 4363–4377.
- (30) Van Vaerenbergh, T.; Fiers, M.; Dambre, J.; Bienstman, P. Simplified description of self-pulsation and excitability by thermal and free-carrier effects in semiconductor microcavities. *Phys. Rev. A* **2012**, *86*, 063808.
- (31) Navarro-Urrios, D.; Capuj, N.; Gomis-Bresco, J.; Alzina, F.; Pitanti, A.; Griol, A.; Martínez, A.; Sotomayor-Torres, C. M. A self-stabilized coherent phonon source driven by optical forces. *Sci. Rep.* **2015**, *5*, 15733.
- (32) Navarro-Urrios, D.; Arregui, G.; Colombano, M. F.; Jaramillo-Fernández, J.; Pitanti, A.; Griol, A.; Mercadé, L.; Martínez, A.; Capuj, N. E. Giant injection-locking bandwidth of a self-pulsing limit-cycle in an optomechanical cavity. *Commun. Phys.* **2022**, *5*, 330.
- (33) Gomis-Bresco, J.; Navarro-Urrios, D.; Oudich, M.; et al. A one-dimensional optomechanical crystal with a complete phononic band gap. *Nat. Commun.* **2014**, *5*, 4452.